Dusty plasma in the vicinity of Enceladus

M. W. Morooka,[1] J.-E. Wahlund,[1] A. I. Eriksson,[1] W. M. Farrell,[2] D. A. Gurnett,[3] W. S. Kurth,[3] A. M. Persoon,[3] M. Shafiq,[1] M. André,[1] and M. K. G. Holmberg[1]

Received 27 July 2011; revised 4 October 2011; accepted 6 October 2011; published 20 December 2011.

[1] We present in situ Cassini Radio Plasma Wave Science observations in the vicinity of Enceladus and in the E ring of Saturn that indicate the presence of dusty plasma. The four flybys of Enceladus in 2008 revealed the following cold plasma characteristics: (1) there is a large plasma density (both ions and electrons) within the Enceladus plume region, (2) no plasma wake effect behind Enceladus was detected, (3) electron densities are generally much lower than the ion densities in the E ring ($n_e/n_i < 0.5$) as well as in the plume ($n_e/n_i < 0.01$), and (4) the average bulk ion drift speed is significantly less than the corotation speed and is instead close to the Keplerian speed. These signatures result from half or more of the electrons being attached to dust grains and by the interaction between the surrounding cold plasma and the predominantly negatively charged submicrometer-sized dust grains. The dust and plasma properties estimated from the observations clearly show that the dust-plasma interaction is collective. This strong dust-plasma coupling appears not only in the Enceladus plume but also in the Enceladus torus, typically from about 20 R_E (~5000 km) north and about 60 R_E (~15,000 km) south of Enceladus. We also suggest that the dust-plasma interaction in the E ring is the cause of the planetary spin-modulated dynamics of Saturn's magnetosphere at large.

Citation: Morooka, M. W., J.-E. Wahlund, A. I. Eriksson, W. M. Farrell, D. A. Gurnett, W. S. Kurth, A. M. Persoon, M. Shafiq, M. André, and M. K. G. Holmberg (2011), Dusty plasma in the vicinity of Enceladus, *J. Geophys. Res.*, *116*, A12221, doi:10.1029/2011JA017038.

1. Introduction

[2] One of Cassini's most exciting results is that the moon Enceladus expels water vapor and ice grains from its south pole and forms a plume [*Dougherty et al.*, 2006; *Spahn et al.*, 2006; *Porco et al.*, 2006; *Waite et al.*, 2006]. A large quantity of ionized gas is produced within both Enceladus plume and dispersed neutral gas, that becomes the major source of plasma for the E ring and the surrounding neutral gas, and provide a dominant plasma source for Saturn's magnetosphere. Heavy ion species were preliminary detected by Pioneer 11, Voyager 1 and 2 [*Richardson et al.*, 1998, and references therein]. Detailed investigation by Cassini confirmed that the plasma of the inner magnetosphere is water dominant [*Young et al.*, 2005]. The heavy, cold, and dense plasma is created within the large toroidal neutral cloud [*Shemansky et al.*, 1993], gradually accumulated until around 5 R_S, and centrifugally transported outward [*Persoon et al.*, 2005].

[3] A mystery of Saturn's magnetosphere has been to relate the planet's rotation period to the dynamics in the magnetosphere and the associated Saturn kilometric radiation (SKR) bursts. More than forty orbits of Cassini observation of the magnetic field could not identify a significant magnetic anomaly [*Burton et al.*, 2009], however, many observations revealed a rotational modulation of the Kronian magnetosphere [e.g., *Espinosa et al.*, 2003; *Gurnett et al.*, 2007; *Burch et al.*, 2008; *Morooka et al.*, 2009]. The periodicities of the magnetosphere can be interpreted as a periodic expanding and a flapping motion of the magnetodisc as the magnetospheric plasma corotates with the planet [*Arridge et al.*, 2008; *Khurana et al.*, 2009; *Morooka et al.*, 2009]. Owing to the variable convection patterns in the neutral atmosphere of Saturn the exact rotational period of the planet is difficult to determine from cloud motions [*Hall*, 1877; *Read et al.*, 2009]. Several Kronian longitudinal systems have therefore been suggested. The SKR longitude system, the most commonly used, is defined using the periodic nature of the radio emissions that originates from the auroral regions of the planet [*Desch and Kaiser*, 1981; *Giampieri et al.*, 2006]. The rotational modulation that has observed closest to Saturn is located in the plasma disk near Enceladus orbit. The electron densities obtained by f_{uh} emission had variation similar to SKR [*Gurnett et al.*, 2007]. Plasma in the Kronian magnetosphere is strongly controlled by the planetary rotation through the magnetic field, which originates from the planet itself [*Blanc et al.*, 2005]. The plasma speed can slow down compared to rigid corotation by, for instance, the continuous supply of plasma through ionization of neutrals near the rings

[1]Swedish Institute of Space Physics, Uppsala, Sweden.
[2]Planetary Magnetospheres Laboratory, Goddard Space Flight Center, Greenbelt, Maryland, USA.
[3]Department of Physics and Astronomy, University of Iowa, Iowa City, Iowa, USA.

0148-0227/11/2011JA017038

and moons. *Gurnett et al.* [2007] suggested that continued ionization around the E ring is responsible for the plasma slippage and convectional electric field pattern fixed to the SKR longitude system, which drives both the modulation and the plasma outflow. The plasma speed observed by ion spectrometers onboard Voyager 1 and 2 and Cassini, so far, is nearly rigid out to 4 R_S and gradually slows down, to 70% of the rigid corotation at the distance of 10 R_S from Saturn [*Wilson et al.*, 2008]. However, this subcorotational plasma flow cannot explain the observed electron density modulation near Enceladus. One concern here is that these particle measurements are not very sensitive to plasma energies below a few eV.

[4] On the other hand, Langmuir Probe (LP) observations, that instead measure the cold plasma (<10 eV) properties, indicate that negatively charged E ring dust causes a slowdown of the plasma in the near equatorial plasma disc [*Wahlund et al.*, 2009]. These observations identified, in addition to the rather hot nearly corotating ion population, a cold (<1 eV) ion population. The amount of the cold ions are significant near the E ring, and their speeds are close to the Keplerian rather than the corotation speed. Closest to the equatorial plane, where the E ring dust is densest [*Kurth et al.*, 2006; *Kempf et al.*, 2008], the ion charge densities were in excess of the electron densities. In space the plasma is "quasi-neutral" and usually the number densities of electrons (n_e) and ions (n_i) are equal. If the plasma contains some dust grains and the electrons are attached to the dust [*Farrell et al.*, 2009], the charge neutrality is determined by the electrons, the ions, and the dust. Such plasma is called the dusty plasma and Saturn's ring region is a place where one can find the dusty plasma in space [*Goertz*, 1989; *Horányi et al.*, 2004]. Except for a few direct measurements in Earth's upper atmosphere [*Havnes et al.*, 1996], there have been no in situ observations of dust-plasma ensembles in space.

[5] During 2008, Cassini performed three Enceladus encounters. Observations by various instruments from these flybys reviled unique characteristics of the plasma environment around Enceladus. Enceladus plume had been inferred in advance from the earlier Enceladus flybys by the magnetic field data [*Dougherty et al.*, 2006]. A large number of water vapor was obtained in the plume [*Waite et al.*, 2006]. Micrometer sized dust grains were detected in and around the plume region [*Kurth et al.*, 2006; *Kempf et al.*, 2008]. Nanometer-size grains that are negatively and positively charged were also confirmed in the Enceladus plume by the electron and ion spectrometers [*Jones et al.*, 2009]. Corotating ions were found to be slowing down before and after the Enceladus encounter [*Tokar et al.*, 2009], and they coincide with the micrometer sized dust and the electron density drop out [*Farrell et al.*, 2009]. These observations are consistent with the idea of dust-plasma interaction by *Wahlund et al.* [2009]: a large number of the electrons are attached to the dust, and thermal ions interact with the negatively charged dust. Recently *Simon et al.* [2011] investigated the effect of the negative charged grains using an analytical model and demonstrated that the charged dust component is necessary to explain the magnetic perturbations observed around Enceladus.

[6] In this paper, we use the data from the Cassini spacecraft of cold plasma properties, to show that the Enceladus southern exhaust plume of neutral gases, after ionization, create a large amount of plasma, and the produced plasma must strongly couple to negatively charged submicron- and micron-sized dust, and decelerate toward the gravitationally affected dust motion. In the following section, we briefly explain the instrument that we used in this paper. In section 3, we show the plasma properties that have been obtained during the Cassini Enceladus encounters in 2008 and discuss the validity of the results. In section 4, we summarize the results and discuss the dusty plasma condition near Enceladus and the E ring. We also suggest that the dust-plasma interaction is the origin of planetary spin modulated dynamics of Saturn's magnetosphere.

2. Instrumentation

[7] We used the data from the Cassini Radio Plasma Wave Science (RPWS) to determine the dusty plasma properties near Enceladus. A full description of the RPWS instrument can be found in the work of *Gurnett et al.* [2004]. One method to obtain the electron density is to use the upper hybrid emission line. The upper hybrid emission peaks in the electric spectra at the upper hybrid resonance frequency $f_{uh}^2 = f_{ge}^2 + f_{pe}^2$ (Hz), where $f_{ge} = 28\ B$ (nT) is the electron gyrofrequency and $f_{pe} = 8980\sqrt{n_e}$ (cm^{-3}) is the electron plasma frequency [*Gurnett and Bhattacharjee*, 2005]. The electron density n_e can be derived from f_{uh} and the magnetic field strength B. The RPWS electric spectra data is also used to detect the micrometer-sized dust [*Kurth et al.*, 2006]. Another method to estimate plasma densities is to use the LP voltage sweep data. The LP sensor is designed to provide in situ information of the ambient plasma. When applying a positive or negative bias potential, the spherical Langmuir probe will attract or repel the electrons and ions from the ambient plasma, and the resulting current is measured. The temperatures and the number density of the electrons and ions in the ambient plasma can be estimated from the probe characteristics. We use a three-electron component theoretical function to fit to the positive voltage part of each sweep to derive the electron parameters, and the negative voltage part gives information of ion drift speed and the ion number density [*Wahlund et al.*, 2009, and references therein] (see also Appendix A), respectively.

3. Observations

3.1. Overall Radio Plasma Wave Science (RPWS) Observations of E03

[8] The third Enceladus flyby (E03, orbit 61) by Cassini occurred on 12 March 2008. The Cassini spacecraft approached Enceladus from the northern hemisphere, across the E ring almost vertically, passed behind the corotation wake of Enceladus, and then through the south pole exhaust plume (see Figure 4a). In Figure 1 we display the Cassini RPWS observations of dust and plasma when the spacecraft moved through +40 R_E to −40 R_E (1 R_E = 251.8 km is the radius of Enceladus) of the equatorial plane of Saturn and past Enceladus. The closest approach (C/A) occurred at 1906:10 UT where the Cassini was at an altitude of 300 km above Enceladus.

[9] Figure 1a shows the dynamic spectrum of electric field emissions sampled by RPWS antenna. A clear narrowband emission close to 80 kHz was detected before and after

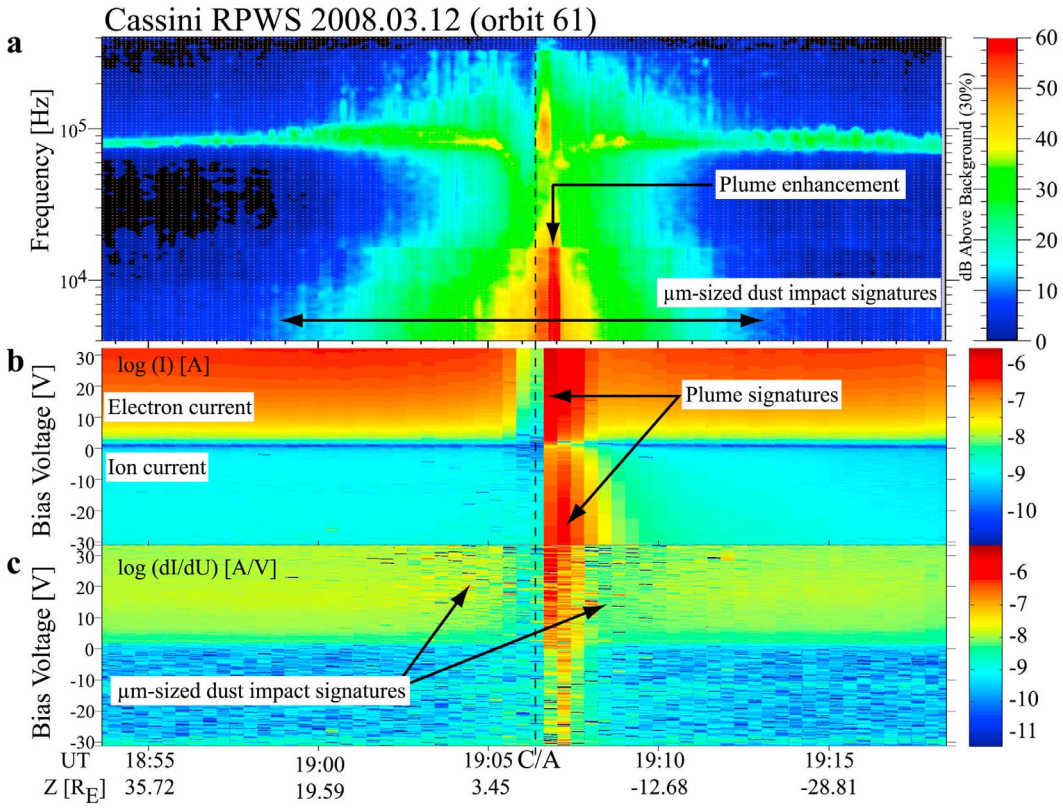

Figure 1. Cassini Radio Plasma Wave Science (RPWS) observations of dust and plasma near Enceladus. (a) Dynamic spectrum of electric field emissions sampled by the 10 m long RPWS antenna, where the spacecraft moved through +40 R_E to −40 R_E from the equatorial plane of Saturn. A clear narrowband upper hybrid emission line near 80 kHz, detected before and after Enceladus encounter, corresponds to a typical plasma disc electron density of about 90 cm^{-3}. A significant drop in the electron density to about 10 cm^{-3} occurs just before closest approach (C/A, 1906:10 UT) of Enceladus. (b) Measured current from bias voltage sweeps of the Langmuir probe. Electrons (sampled at positive bias voltages) and ions (sampled at negative bias voltages) are measured independently. (c) The derivative (dI/dU) of the voltage–current characteristic of the Langmuir probe.

Enceladus encounter, and interpreted as the upper hybrid (f_{uh}) emission line. The frequency of the f_{uh} corresponds to a typical plasma disc electron density of ≈90 cm^{-3}. Broadband emission across all frequencies were observed from 1858–1913 UT. This is at least partly due to impacts of micrometer-sized dust in the E ring on the spacecraft and RPWS antenna [*Kurth et al.*, 2008; *Wang et al.*, 2006]. From the trajectory information of Cassini, it is revealed that the micrometer-sized dust is detected by the RPWS antenna about ±20 R_E from the equatorial plane and peaks in the Enceladus plume (1906–1907 UT). The upper hybrid line significantly drops just before C/A, indicating that the electron density decreased to ≈10 cm^{-3}. However, the emission was obscured by the broadband emissions due to dust impacts and the f_{uh} line was difficult to identify near C/A. This feature has been previously reported by *Farrell et al.* [2009], who suggested that the electron density decreases due to the electron attachment to dust grains smaller than the μm sized dust grains measured by RPWS. *Farrell et al.* [2009] calculated the electron loss process for the Enceladus flyby and concluded that water-ion recombination and water molecule dissociation cannot explain the electron's density decreasing but the electron absorption to the dust.

[10] Figures 1b and 1c display the measured LP current from the bias voltage sweeps and their derivatives (dI/dU), respectively. Dust impacts are detected also by the LP as sharp spikes (noise) mostly for positive bias voltages from 1902–1911 UT (most easily detected in the derivative; Figure 1c). By sampling the current for the negative bias voltage (ion side) and the positive bias voltage (electron side), the LP can measure the density of ions and electrons independently. The plume is clearly detected as enhancements in both electron and ion currents from 1906:30 UT to beyond 1910 UT (Figure 1b), which are mainly due to the electron and ion density enhancements, respectively. During C/A, when the spacecraft traversed the ideal corotation wake of Enceladus, the electron current dropped, while the ion current was largely unaffected.

3.2. Langmuir Probe Sweep Analysis

[11] *Wahlund et al.* [2009] reported that the number density of the electrons is smaller than the ion density within the center of the E ring where μsized dust was detected by both RPWS and CDA [e.g., *Kurth et al.*, 2006; *Kempf et al.*, 2008]. The density difference between the ions and electrons can be significant especially in the Enceladus plume,

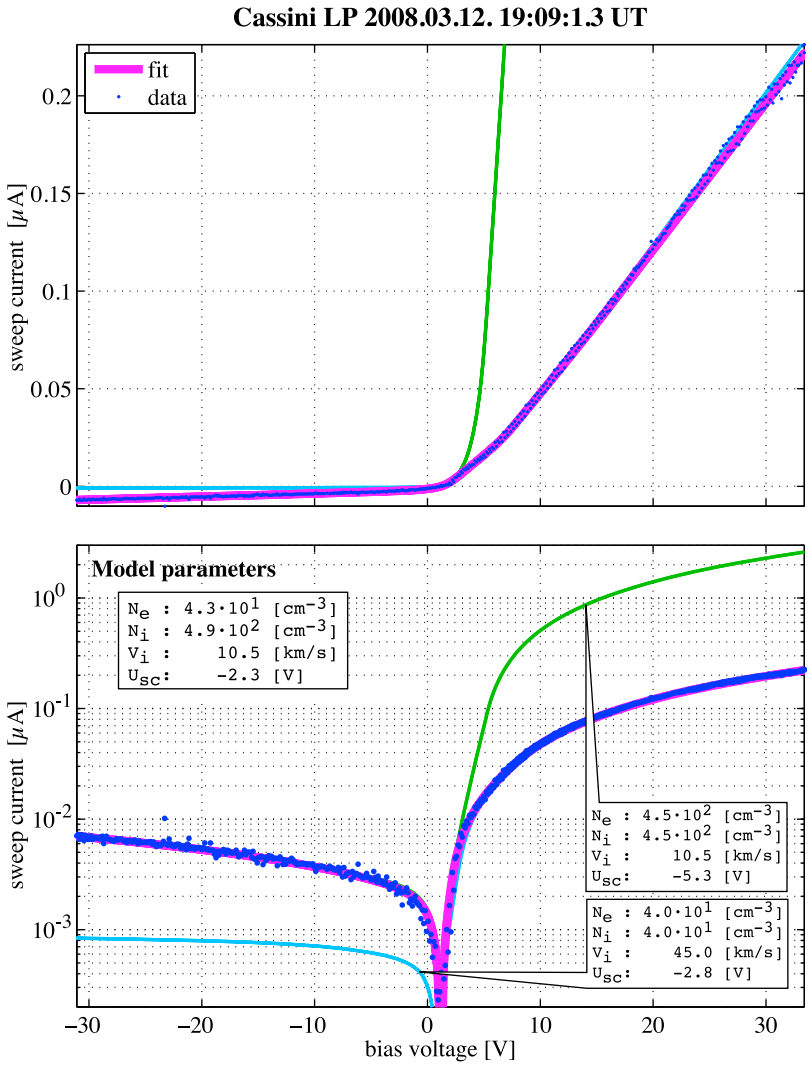

Figure 2. The Langmuir Probe (LP) sweep current obtained in Enceladus plume region in (top) linear scale and in (bottom) logarithmic scale. The blue dots are the observed data points. These points are fitted to a theoretical model (magenta line) to obtain the plasma parameters displayed at the upper left of Figure 2 (bottom). The parameter shows large differences between the ion density and electron density. The light blue line is the model current with setting the ion density to the same value as the electron density. The model current in the green line instead uses the observed ion density as the electron density.

that is a major source of the E ring dust. Figure 2 shows an example of the LP sweep current characteristics obtained far out in the Enceladus plume region (1909:01 UT). The blue dots are the measured current displayed in linear scale (Figure 2, top) and logarithmic scale (Figure 2, bottom). The theoretical sweep fits used in Figures 2 and 3 assume the ions consist mainly of water (amu = 18), but fits with both water group and hydrogen ions have been investigated. The best fitted function to the sweep data is plotted in magenta lines. The inferred electron and ion parameters from this fitting are displayed in the box at upper left corner in Figure 3b, and indicates a large density difference between the electrons and ions. The electron density is 43 cm^{-3} while the ion density is 490 cm^{-3}, which is an order of magnitude larger than the electron density. Since quasi-neutrality must be maintained, this difference can be attributed to the existence of the negatively charged small dust particles. As we see in Figure 1, there was a detection of μm sized dust grains, where each such grain typically attaches thousands of electrons [*Horányi et al.*, 2004].

[12] The green lines in Figure 2 are the theoretical current when the total electron density is set to the same value as the measured ion density. The observed electron current is clearly smaller by an order of magnitude compared to the modeled current. This effect is consistent with Langmuir probe measurement of dusty plasma in the laboratory [e.g., *Barkan et al.*, 1994].

[13] The model current here consists of (1) the current from the ambient electrons, (2) the current from the ambient ions, and (3) the current of the photoelectrons escaping from the probe. When the probe is inserted into the dusty plasma there are also other current sources that need be taken into account. The secondary electron emissions due to dust impacts can increase the current on the ion (negative voltage) side in a

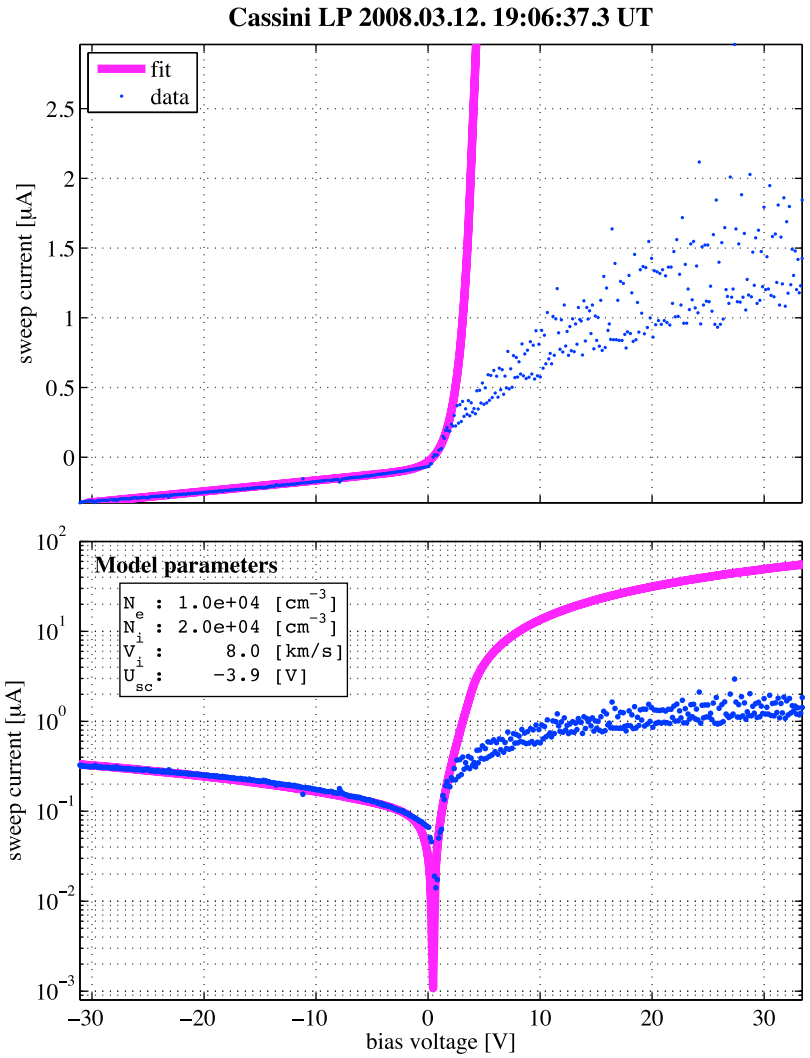

Figure 3. The LP sweep current obtained just after the spacecraft was inserted into the central plume region. The electron current saturates at the bias voltage above a few volts.

similar manner as photoelectrons from the probe do [e.g., *Horányi*, 1996]. The dust impacts can create current on both ion and electron side. However, usually the electron charging dominates because the thermal speed of the electron is much higher than that of the ions [e.g., *Shukla and Eliasson*, 2009].

[14] On the negative bias voltage side, the current from the ambient ions and dust becomes

$$I_i = -\frac{1}{4}Aq_+n_+v_+\left(1-\frac{2e}{m_+v_+}(U_{SC}+U_{bias})\right), \qquad (1)$$

where A is the surface area of the probe, n_+, m_+, and v_+ are the number density, mass and the velocity of ion or dust, U_{SC} and U_{bias} are the spacecraft potential and the bias potential to the probe. The dust can be counted as heavy negative ions. For any high-energy positively charged particle, the second term in the bracket of equation (1) becomes very small and the result current would be constant. Therefore only the current by cold ions will cause a gradient. Since a significant gradient has been observed on negative voltage side near the Enceladus (Figure 2), the observed region must be dominant by the cold thermal ions and the current from heavy dust grains must be small. The estimation of the ion velocity can be under estimated if the dust current is not taken in account, and this error could be up to 30%. These effects are discussed in Appendix A. The blue line is the model current when the ion number density is set to the same value as the electron density. The modeled value is actually comparable to the photoelectron current from the probe in the region, and therefore negligible. This would require some 10 nA current due to secondary electrons from dust impacts on the negative voltage side. However, the secondary electron current for negative voltage bias is a constant, and cannot explain the shape of the measured sweep characteristic while a thermal cold ion population can. We therefore conclude that the large measured current on the negative voltage side is predominantly due to a cold ion population. The ion drift speed of the blue line in Figure 2 is set to a larger value corresponding to the local corotation speed. Note that this model current results in a constant current on the negative voltage side, which is expected from equation (1). Lower drift speeds would result in even smaller currents, and would not change

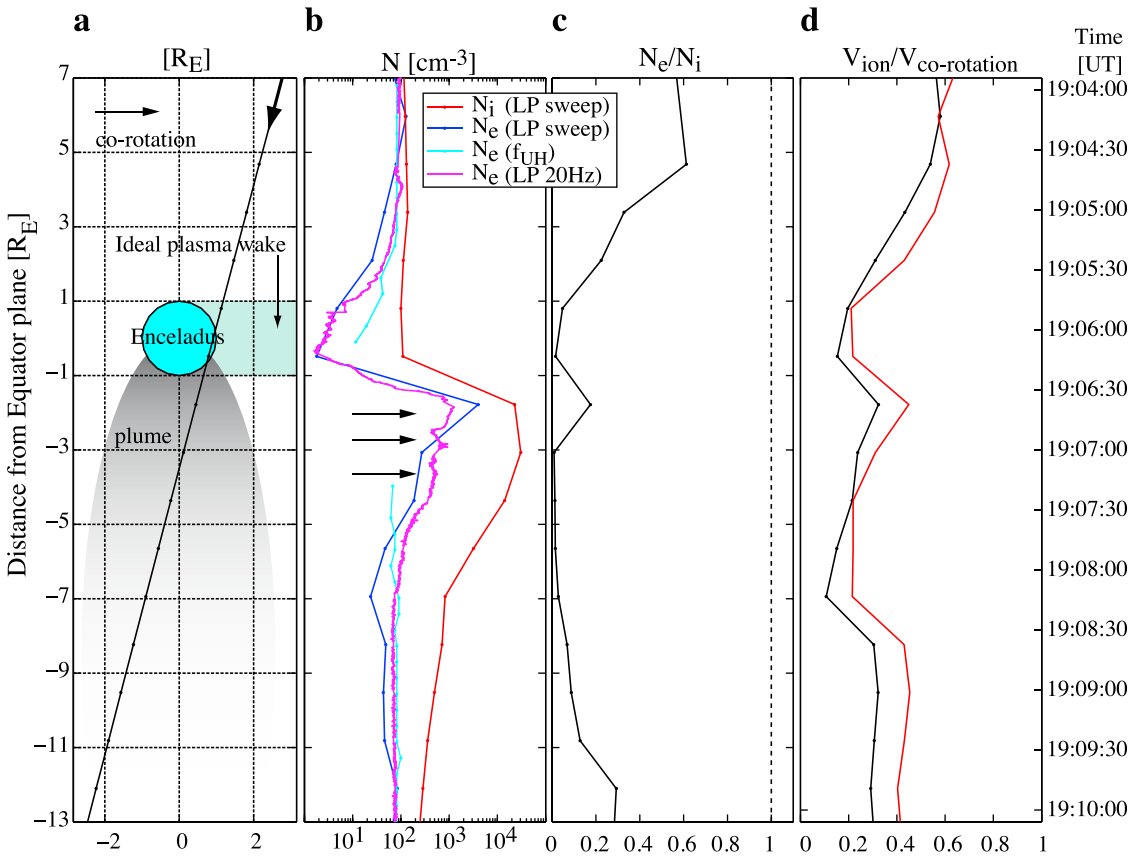

Figure 4. Flyby geometry and derived cold plasma parameters of the Enceladus E03 encounter. (a) Spacecraft trajectory flyby geometry in the frame of Enceladus. The corresponding observation times are displayed in Figure 4d. (b) Plasma densities estimated from several RPWS techniques. Several electron density peaks in the plume are detected in the 20 Hz Langmuir probe data (magenta), which correspond well with the footprint of "tiger stripes" (3) exhaust structures (arrows). (c) The LP electron to ion density ratio showing a significant depletion of electrons during the flyby. (d) The solid line is the ratio of the observed ion speed to the rigid corotation speed, both in the spacecraft frame of reference. The ion speed is inferred from the LP ion flux measurements assuming water group ions. The red line is the corrected ion speed relative to the corotation speed using equation (A12).

the above conclusion. The effect of photoelectrons from the spacecraft is small in this negative spacecraft potential region, and rather would affect the positive biased voltage side (electron side).

[15] Figure 3 shows another LP sweep current example, in this case obtained just after Cassini was inserted into the central plume region (1906:37 UT). The LP sweep current trails off for bias voltages above a few volts positive (i.e., reach electron current saturation). Reaching such a limiting current by the LP saturation means that, indeed, a cold and very dense electron plasma is encountered.

[16] The saturation current is given by

$$I_{e,\mathrm{sat}} = en_e A_{\mathrm{LP}} \sqrt{\frac{eT[\mathrm{eV}]}{2\pi m_e}}, \qquad (2)$$

where $A_{\mathrm{LP}} = 4\delta r_{\mathrm{LP}}^2$ is the probe area and r_{LP} the probe radius. Taking the electron saturation current of 1–2 μA and assume that the electron temperature is one eV, we obtain an electron density of 4.8–9.5 $\times$ 10^3 cm^{-3}. The value is consistent with the electron density using the electron fitting method with values shown in the box. The result is only weakly dependent on the electron temperature. The fact that the saturation starts close to the floating potential (near +1 V) means that the electron sampling region around the LP sensor is small, and that the electrons are affected collectively within a short Debye length.

3.3. Encounter E03

[17] Figure 4 shows the plasma parameters obtained along the Cassini trajectory during the E03 encounter past Enceladus. All data are plotted along the Z direction in the Enceladus corotation coordinate system, i.e., the distance from the equatorial plane in Enceladus radii (R_E). The trajectory of the Cassini is plotted in Figure 4a. The horizontal axis in Figure 4a is the X axis of the Enceladus corotation coordinate system, that is toward the rigid

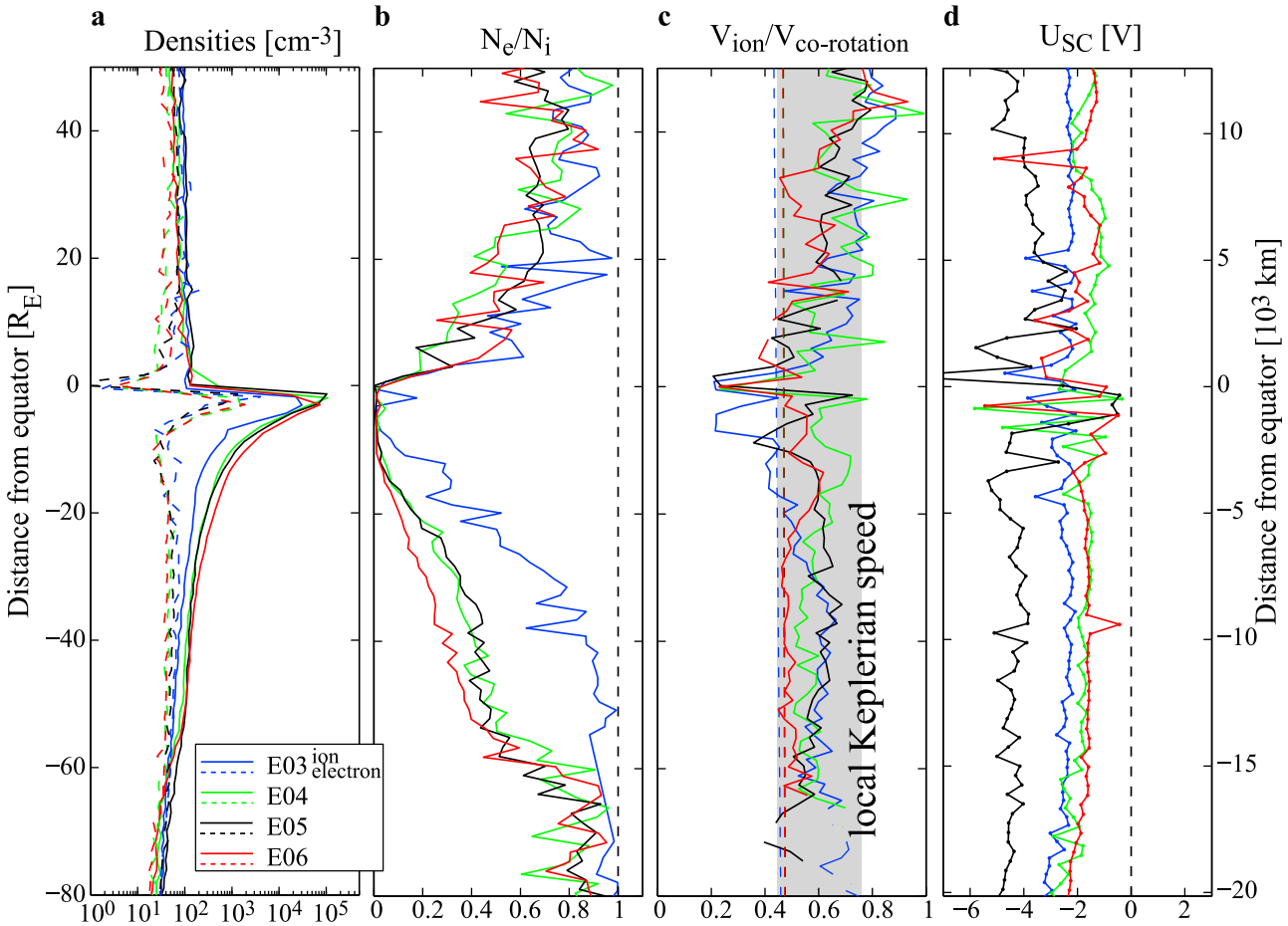

Figure 5. Plasma disc characteristics around a wide region around the E ring and Enceladus. The four Enceladus encounters E03–E06 had similar trajectories past the moon, and the cold plasma parameters have similar consistent characteristics. Each flyby is indicated with colors displayed in the label. (a) LP electron (solid line) and ion (dashed line) densities. (b) The electron to ion number density ratio. (c) Ratio of the ion speed to the rigid corotation speed. The ion speed is collected using equation (A12). (d) The spacecraft potential (U_{SC}), which is to be a proxy for the charge of the water-rich dust grains.

corotation. Figure 4b shows the electron and ion densities estimated by the LP sweep analysis together with the electron density estimated from the upper hybrid emission line. Overall the LP observed electron density is consistent with the value derived from f_{uh}. Clearly all the densities became large when the spacecraft crosses the central plume region ($-1\ R_E < Z < -7\ R_E$). The densities of ions and electrons reach 30,000 cm^{-3} and 4000 cm^{-3}, respectively, based on the LP measurements. These large plasma densities in the plume are expected from combined photoionization by solar EUV radiation and impact ionization by hot plasma of the plume neutrals that in balance with the recombination and electron attachment of electrons with water molecules (compare section 4). Comparably, neutral water molecule densities have been reported to be 5×10^7 cm^{-3} near the center of the E03 plume, decreasing to 10^4 cm^{-3} far outside the plume [*Waite et al.*, 2006].

[18] Figure 4c displays the electron density to the ion density ratio (n_e/n_i) derived from the LP sweep data. The electron densities were found to be 1–2 orders of magnitude smaller than the ion densities in a larger region around Enceladus (Figures 4b and 4c). The ratio n_e/n_i is smaller than 1 not only in the region shown in Figure 4 but also continues beyond $-13\ R_E$ below the equatorial plane far out in the Enceladus plume (see Figure 5b). The ratio n_e/n_i becomes less than 0.01 in the center of the plume, i.e., 99% of the negative charges are missing.

[19] The 20 samples/s continuous LP current data (with fixed voltage bias) revealed structured density peaks in the plume region (Figure 4b, magenta). The times when Cassini was above the footprints of the Enceladus tiger stripes [*Jones et al.*, 2009] are marked with arrows. Thus, the electron density peaks can be the local ionization enhancement due to local neutral gas enhancements caused by the individual plume sources.

[20] Figure 4d shows the ion speed inferred from the LP (solid line) in units of the local rigid corotation speed. The plasma in Saturn's magnetosphere tends to be picked up and corotates with the planetary magnetic field by the action of an induced corotation electric field ($\mathbf{E}_{rot} = -\mathbf{v}_{corotation} \times \mathbf{B}$). The rigid corotation speed relative to the spacecraft is ≈32.5 km/s near Enceladus orbit. However, the LP inferred

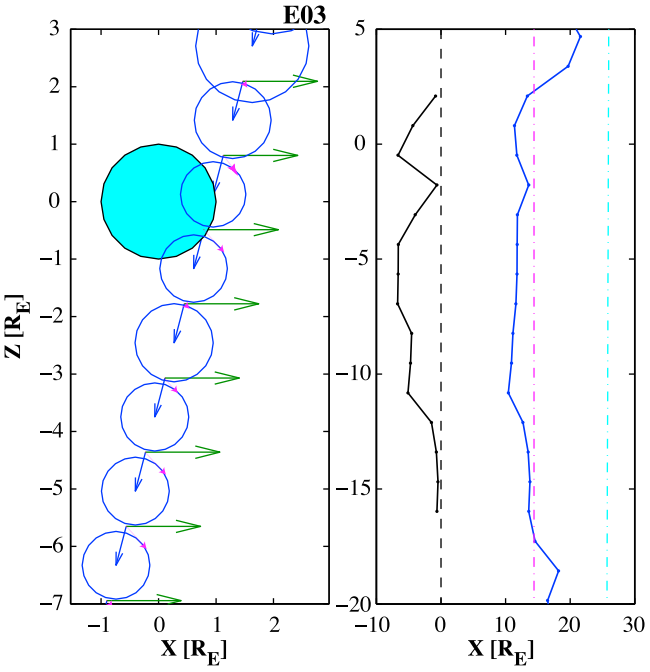

Figure 6. (left) The relationship between the spacecraft velocity and obtained ion speeds in the *XZ* plane of the Enceladus corotation coordinate. The blue arrow shows the spacecraft velocity vector. The size of the circles represents the observed ion speed centered at the end of the spacecraft velocity vector. Then the ion velocity vectors should start from the start point of the spacecraft vectors and end somewhere on the circle. The green vector represents the rigid corotation for comparison. (right) The solid line shows the minimum required vertical ($-Z$ directed) ion velocity. The blue line is the observed value of the total ion speed. The vertical dashed lines are the Keplerian (magenta) and the corotation (light blue) speed, respectively.

ion speeds were less than half the corotation speed in the whole observed region, and were instead close to the local Keplerian speed (≈14.5 km/s, relative to the spacecraft speed, $v_{\mathrm{ion}}/v_{\mathrm{corotation}} \approx 0.4$), suggesting that the plasma around Enceladus was moving with a similar speed as Enceladus itself. The v_{ion} can be under estimated if the negatively charged dust current is not taken in account (see section A2). The red line is the corrected ion speed when counting on the dust ram current using equation (A12). Here we assume that the ions are corotating while the dust has Keplerian speed ($\hat{a} = v_d/v_i \approx 0.4$) and the observed ion/electron densities are used to derive $\acute{a}$ using equation (A5). It is shown that the ion speed is still much lower than the corotation speed.

[21] The LP ion current can be fully written as

$$I_i = -Aq_i n_i \sqrt{\frac{v_i^2}{16} + \frac{k_B T_i}{2\pi m_i}} \left(1 - \frac{2e(U_{\mathrm{SC}} + U_{\mathrm{bias}})}{(m_i v_i^2 + 2k_B T_i)}\right). \quad (3)$$

Owing to a significantly large spacecraft ram speed it is usually reasonable that the ion bulk speed current dominate over the thermal component. In this case the observed ion speed can be regarded as a upper limit of the ion thermal speed T_i. In the E ring region, the ion speed in the moon frame was ∼5 km/s. This leads to the water group T_i of <17 eV. In the Enceladus plume region a local acceleration in $-Z$ direction is expected (see section 4.3 and Figure 6) [see also *Farrell et al.*, 2010]. Then the ion thermal speed must be much smaller than the observed drift speed. This is consistent with a cold ion component reported by *Wahlund et al.* [2009].

[22] A plasma moving with a nearly Keplerian ion speed is consistent with the observed density characteristics in the presumed wake of Enceladus (Figures 6a and 6b). When a solid obstacle is situated in a fast flowing plasma ($v_i > c_s$, the local ion sound speed) a wake will be created behind the obstacle and the ion density will decrease, while the mobile electrons tend to diffuse rapidly into the wake. However, ion densities just before the plume region are largely unaffected (near 100 cm^{-3}) within the ideal wake, while the electrons are depleted down to a few cubed centimeters. This observed behavior is inconsistent with a developed wake. It is rather an effect of electron attachment to E ring dust particles from a plasma not moving relative to Enceladus.

3.4. The E03, E04, E05, and E06 Encounters

[23] During 2008, there were three other Enceladus encounters (E04–E06), which had similar trajectories. Figure 5 shows the comparisons of the plasma parameters obtained by LP for all four flybys. Clearly, the characteristics of the electrons and ion densities as well as the ion velocities were found to be consistent for all flybys. First, both electron and ion densities became large within the Enceladus plume region. In the center of the plume densities reached 30,000–100,000 cm^{-3} for the ions and 2000–4000 cm^{-3} for the electrons (Figure 5a). Second, the electron densities are significantly smaller than the ion densities ($n_e/n_i < 0.01$) in the Enceladus plume region. The n_e/n_i ratio was low (0.7–0.8) also in a larger region in Z at +20 R_E to −60 R_E (Figure 5b). In this respect the E03 encounter deviated somewhat compared to the other flybys in the southern hemisphere. This could be due to Cassini crossing the equator shallower during E03 compared to other orbits. The Cassini orbit of E04–E06 crossed the equator more vertically. And last, the ion density was nearly constant just before the plume encounter (0–10 R_S) and no plasma wake signature was detected (Figure 5a), indicating that the surrounding plasma moves with a similar speed as Enceladus. Also consistently, the ion speed is overall slower than the rigid corotation speed and close to Keplerian speed in a large region from −60 R_S to +20 R_S (Figure 5c).

[24] Although the observed ion speeds presented here clearly depart from the local plasma rigid corotation speed and are rather Keplerian in character, the values are not constant. In Figure 5c, one can see a trend in the ion speed with a local minimum around the Enceladus plume where the values become even smaller than the Keplerian speed. If one considers the plasma motion in the Enceladus rest frame, an observed slower ion speed indicates the ions have a velocity component directed in toward the negative Z direction (i.e., away from Enceladus in its southern plume hemisphere). The LP can only determine the absolute value of the ion speed in the spacecraft velocity frame. When the observed ion speed is smaller than the spacecraft speed, the

Table 1. Typical Dusty Plasma Parameters Obtained From Enceladus Flybys[a]

	Enceladus Plume	E Ring (Near Enceladus)
n_e (cm^{-3})	300	80
n_i (cm^{-3})	30,000	100
T_e (eV)	2	2
U_{SC} ($\approx U_d$) (V)	−3	−2
n_d (cm^{-3})	95	0.25
d (cm)	0.13	0.98
$\ddot{e}_d$ (cm)	6.04	78

[a]The electron density (n_e), the ion density (n_i), the electron temperature (T_e), and the spacecraft potential (U_{SC}) are the values observed by RPWS/LP. The dust density (n_d), the intergrain distance (d), and the dust Lamor radius ($\ddot{e}_d$) are calculated from the observed values. Equation (1) is used to calculate n_d.

ions would have a velocity component in the direction of the spacecraft trajectory.

[25] Figure 6 (left) shows an example of the relationship between the spacecraft velocities and ion speed obtained from E03. The blue arrows show the spacecraft velocity vectors for each LP sweep sample position in the *XZ* plane, and each circle represents the required end position of the ion velocity vector inferred from the observed LP ion speed value. For comparison, the green arrows are the rigid corotation velocity vectors in the Enceladus rest frame. Since the Cassini's trajectories of the Enceladus flybys were rather steep into the equatorial plane, the ions are required to have a velocity component in negative *Z* direction. The minimum required vertical ion speed in the *Z* direction is shown in Figure 6 (right) (solid line). Clearly such a downward component of 5–10 km/s (10–20 eV for water group ions) near Enceladus is required from the LP ion speed measurements. That would correspond to an electric field of about 3–4 μV/m, if directed along the magnetic field. This feature is consistent with the CAPS/IBS observations of a dispersion of the ion distribution, which *Farrell et al.* [2010] suggests is due to an electric field in *Z* direction built up by charged dust grains within the Enceladus plume region. For comparison, the blue line in Figure 6 (right) shows the inferred total ion speed from the LP sweep measurements.

[26] Figure 5d shows the spacecraft potential, U_{SC}. Even though the E ring dust grains and the Cassini spacecraft consist of significantly different materials, they are exposed to the same charging mechanisms. Therefore, we can use U_{SC} as a proxy of the potential of the dust grain [*Kempf et al.*, 2006; *Wahlund et al.*, 2009]. U_{SC} is a few volts negative during the whole observed region, consistent with the result that the dust grains are negatively charged.

4. Summary and Discussion

[27] The Langmuir Probe observations from the four Enceladus encounters during 2008 revealed the cold plasma and charged dust characteristics in the vicinity of Enceladus. All data showed consistent characteristics as follows.

[28] The existence of a large amount of plasma (30,000–100,000 cm^{-3} for ions and 2000–4000 cm^{-3} for electrons) that must be a result of the ionization of the observed neutrals in the Enceladus plume [e.g., *Waite et al.*, 2006].

[29] Existence of a large amount of micrometer-sized, and inferred nanometer-sized, dust grains that attach the surrounding electrons and becomes predominantly negatively charged.

[30] The LP inferred bulk ion speeds are significantly smaller than local rigid corotation speed and rather Keplerian in character, indicating that the surrounding plasma is moving at nearly the same speed as the moon Enceladus and the surrounding dust (E ring and plume). In this case the expected wake effect of the moon on the ion density would not be observed. Our measurement of ion number density in the "ideal wake region" was unaffected, i.e., consistent with the LP ion speed estimation.

4.1. Dusty Plasma Characteristics

[31] The plasma observed here contains, in addition to the electrons and the ions, charged dust that ensures charge quasi-neutrality. Such plasma is called dusty plasma where the intergrain distance (dg) is smaller than the plasma Debye length ($\ddot{e}D$). Dust can be regarded as an isolated particle when $dg > \ddot{e}D$ and is then instead called a dust in plasma [e.g., *Shukla*, 2001]. In dusty plasma, the Debye screening of the plasma shields the Coulomb field of an arbitrary charge, and the dynamics of the charged dust and plasma becomes collective. The dusty plasma parameters for typical Enceladus plume and E ring condition, as presented here, are shown in Table 1. The dust density n_d and the intergrain distance, $d_g \equiv (3/4\eth n_d)^{1/3}$, is estimated using *Yaroshenko et al.* [2009, equation (6)]:

$$n_d \cong \frac{q(n_e - n_i)}{q_{\min}} \frac{2-\mu}{1-\mu}, \tag{4}$$

where $q_{\min} = 4\eth\mathring{a}_0 U a_{\min}$. U is the electric potential of the grain and we use the spacecraft potential, U_{SC}, obtained by the LP. We assume here that the size distribution of the dust, described by the function $W(a)$, is proportional to $a^{-\mu}$, where a is the radius of dust and μ is set to 4 based on CDA observations [*Kempf et al.*, 2008]. For very small nanometer-sized grains, as observed by CAPS/ELS [*Jones et al.*, 2009], the equilibrium charge is fraction that causes individual grain charge to be positive and negative at times. On the other hand, larger sized grains, submicrometer to micrometer grains, can have large amount of charges (typically thousands of charges). The dust charges observed here is the bulk charge of such nanometer- and micrometer-sized dust ensemble. Also the smallest dust grain radius, $a_{\min}$, is set 0.1 μm for this calculation. However, $a_{\min} = 0.1$ μm is far larger than the 1 nm sized dust grains observed by *Jones et al.* [2009]. The dust number density and charge density considering also the small size dust distribution in the E ring and the Enceladus plume must be studied elsewhere in the future. The obtained value of d_g is clearly smaller than the local plasma Debye length both in the plume region and in the E ring.

[32] *Havnes et al.* [1990] introduced a number that can represent the collective order of the dusty plasma, called "Havnes parameter":

$$P_H = \frac{kT}{en_p} \int aW(a)da, \tag{5}$$

where n_p is the density of the ambient plasma and n_i can be used here.

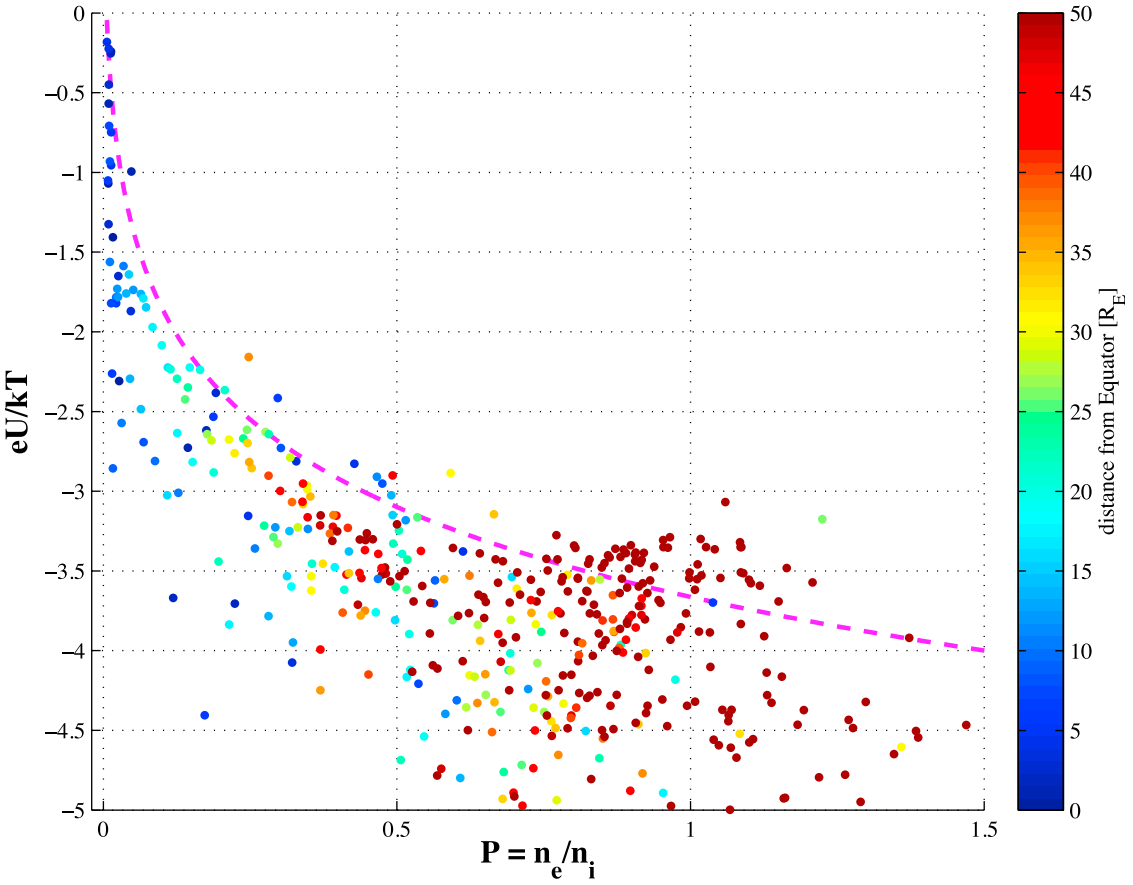

Figure 7. The magenta dashed line shows the relationship between n_i/n_i (P) and the dust grain potential for amu = 18 ion plasma. When the P becomes small, the potential difference between the dust grain and the ambient plasma becomes small, and the dusty plasma is collective. Very small values of P ($P \approx 0$) lead to zero grain potential, and the electrodynamics of the dust no longer appear. The color-coded dots are the parameters obtained during the four Enceladus flybys. The color indicates the distance from the equator plane. The observed environments in plume (dark blue color) and E ring (light blue to yellow) are both collective dusty plasma.

[33] From the charge balance of the local dusty plasma and the current balance into the dust grain,

$$e(n_i - n_e) = \rho_d, \tag{6a}$$

$$I_i = I_e, \tag{6b}$$

$$\rho_d = 4\pi\varepsilon_0 U \int aW(a)da = q(n_i - n_e), \tag{6c}$$

$$I_i = en_i\sqrt{\frac{kT}{m_i}}\left(1 - \frac{eU}{kT}\right)\pi a^2, \tag{6d}$$

$$I_e = en_e\sqrt{\frac{kT}{m_i}}\exp\left(\frac{eU}{kT}\right)\pi a^2, \tag{6e}$$

it is possible to show a universal relationship that gives the variation of the dust potential to the plasma eU/kT respect to P [*Barkan et al.*, 1994]:

$$\sqrt{\frac{m_i}{m_e}}\left(1 + \frac{4\pi\varepsilon_0}{e}P_H\frac{eU}{kT}\right)\exp\left(\frac{eU}{kT}\right) + \left(1 - \frac{eU}{kT}\right) = 0. \tag{7}$$

The Havnes parameter P has a unit of m V while eU/kT is dimensionless. For convenience, we use instead simplified number:

$$P = \frac{1 - \rho_d}{n_i} = \frac{n_e}{n_i}. \tag{8}$$

Then equation (6) becomes

$$\left(1 - \frac{eU}{kT}\right) + P\sqrt{\frac{m_i}{m_e}}\exp\left(\frac{eU}{kT}\right) = 0. \tag{9}$$

A similar relationship can also be found in the textbook of the dusty plasma [*Shukla and Mamun*, 2002]. Figure 7 shows this relationship of the parameter P and the dust potential eU/kT for the water group ion plasma ($m_i = 18\ m_H$). The dashed magenta line is the solution of equation (8), which assumes a negligible photoelectron current from the grain, which is mostly a good assumption when comparing ambient plasma currents with the photoelectron contribution to the LP probe current for negative voltage bias.

[34] When P is close to 1 the dust grain can be regarded as isolated in the plasma, and its electric potential becomes

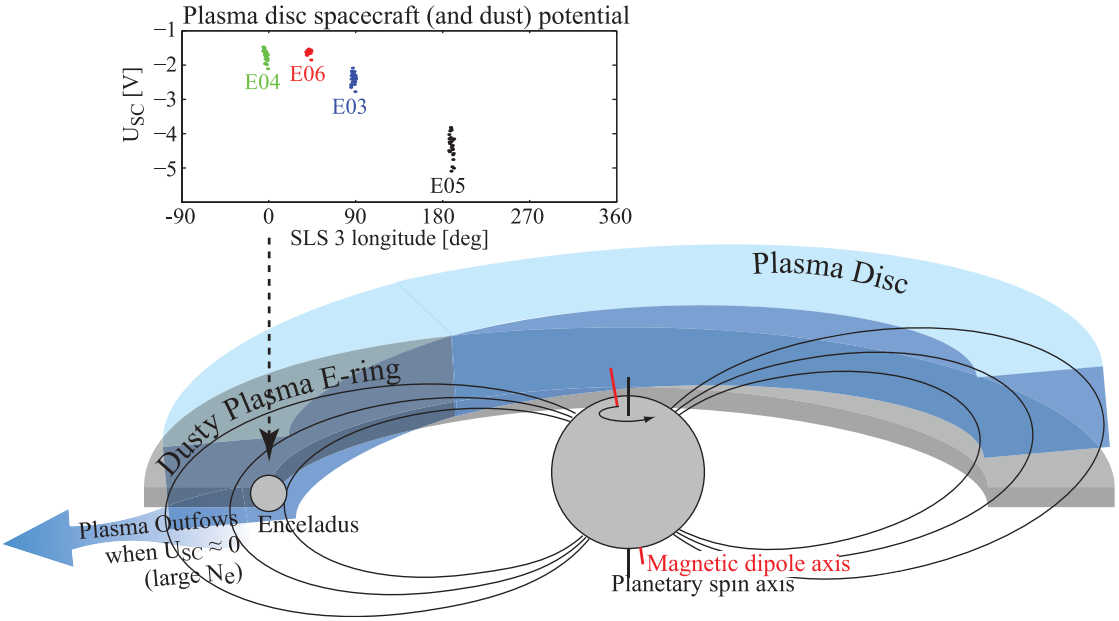

Figure 8. The interrelationship between the E ring of charged dust and the plasma disc. The cartoon illustrates how the plasma disc interacts with the E ring when the planetary magnetic dipole axis is slightly tilted and northward shifted compared to the planetary spin axis. The plasma disc center will join with the E ring dust disc center at a certain longitude in the Saturn Longitude System (SLS) rotating system. At this point, the densest plasma exists and associates with the least negative spacecraft potentials (shown in dashed arrow). Plasma outflows are prone to occur at this certain position, where the dust grains are least negative and their electrostatic grip on the ion population is the least. Spacecraft potentials in the surrounding plasma disc from the four Enceladus encounters are plotted in the upper right. A clear relationship between U_{SC} and the SLS longitude is consistent with the idea.

constant. On the other hand, when P becomes very small the electric potential of the dust reaches zero. The dusty plasma is efficiently collective when P is less than 0.5. The dots in Figure 7 (using the LP inferred electron temperature, spacecraft potential, and the difference in electron and ion number densities) represent observed values obtained during the four Enceladus flybys during 2008, where the spacecraft was within 100 R_E from the equator plane. It is worth noting, that the calculation does not need an assumption of the particular dust distribution, just the integrated charge on the dust population. The color of the data points express the distance from the equator plane in unit of R_E. It is clearly shown that most data points follow the theoretical line in the range of $P < 0.5$, indicating that the dust-plasma dynamics is highly collective. The dark blue colored dots (i.e., close to Enceladus) exist around $P = 10^{-2}$. Many data samples in the range of $P < 0.5$ are obtained even beyond a distance of 10 R_E from the equator plane. This means that the collective dynamics of dusty plasma is important not only in the Enceladus plume region, but also in the plasma torus surrounding the E ring. This condition is consistent with our observation that the surrounding plasma is moving near Keplerian speed with the charged dust. Also the electron current saturation in the plume (Figure 3), showing that the potential between the ambient plasma and the probe must be small, suggests that the Debye sheath around the probe is small. Such dusty plasma must be collective. At the far distance from the equator plane (where the data points are marked in red), the Havnes parameter, P, at times becomes close to 1 and the plasma starts to move out from the collective regime. The data points are also scattered off from the theoretical line for these P values, which is probably due to a small dust density, inaccuracy in the inferred difference between n_i and n_e and/or that the photoelectron or secondary electron currents becomes important compared to the ambient plasma currents in a thin plasma.

4.2. Dynamics of the Dusty E Ring and Plasma Disc

[35] The observed electrodynamic coupling of the plasma and dust implies a relationship between the "gravitational" moving magnetospheric plasma (plasma disc) and the SKR modulation. Saturn's magnetic dipole may have a very slight tilt and a northward shift compared to the planet's spin axis, which makes the magnetodisc plasma wobble with respect to the E ring [*Goertz et al.*, 1981], and the interaction with the dusty plasma of the E ring will be enhanced once each planetary spin period (Figure 8). An indication that this takes place is a modulation of the predominant dust potential (Langmuir probe inferred spacecraft potential, U_{SC}) in one planetary spin period. U_{SC} is in this region a function of the electron density and temperature of the surrounding plasma. A dense and cold plasma drives U_{SC} toward positive, and vice verse. Therefore one can track the plasma disc rotation by monitoring the spacecraft potential. There is a clear relationship between the spacecraft potential of the plasma disc and the longitude of the rotating Saturn Longitude System [*Kurth et al.*, 2008]. This is mostly due to a reported similar variation of the electron density in the plasma disc

[*Gurnett et al.*, 2007]. The center of the plasma disc where the densest plasma exists is associated with the least negative spacecraft potentials. The dust potentials becomes positive at a radial distance of about 7–8 Saturn radii, and this will occur closest to the plasma disc near 0° SKR longitude. At this point the plasma is most prone to be released by the electrodynamic coupling of the dust and start to flow outward to the surrounding magnetosphere at a specific SKR longitude, and there creates a spiral pattern of cold plasma. The magnetic equator was observed to have a northward shift of about 0.036 R_S [*Burton et al.*, 2009]. With this amount of shift and at least 0.07° of dipole tilt from the planetary spin axis, the magnetic equator plane and the geodetic equator plane cross each other around the Enceladus every planetary spin period. As the plasma disc center approaches to the E ring, denser plasma surrounds the E ring dust grains, the dust potential tends to become least negative. This must be the region that the ions are released from the dust potential and the electron density around the Enceladus becomes large (near 0 SKR longitude). A large amount of data from the plasmadisc region by the Cassini can bring further information of the dusty plasma dynamics in detail.

Appendix A: Langmuir Probe Data Interpretation

[36] It may seem that straightforward analysis of Langmuir probe data may be called into question in a plasma with such a large part of the negative charge bound to dust as our results imply. In this appendix, we discuss the analysis, and find that the dust changes the applicable probe theory only slightly.

A1. Probe Currents

[37] The fundamental parameter measured by the spherical Langmuir probe on Cassini is the current it collects, which by convention is set as positive when the current flows from the probe to the plasma. This current depends on the potential of the probe to the surrounding plasma, U_p. The controllable voltage is the bias voltage U_{bias} applied to the probe, which relates to U_p by

$$U_P = U_{\mathrm{SC}} + U_{\mathrm{bias}}, \tag{A1}$$

where U_{SC} is the spacecraft potential with respect to the plasma. The operational mode of primary interest here are the probe bias sweeps, where U_{bias} is varied in a series of steps during a short time. Examples of sweeps can be seen in Figures 2 and 3.

[38] The current to the probe is carried by plasma particles, charged dust, and electrons emitted from the probe by photoemission and secondary emission. Secondary emission is important only in regions with significant keV particle fluxes and is ignored here. The photoemission current is very small compared to the ion and electron currents we detect and can be safely neglected.

A2. Ion and Dust Velocity

[39] The remaining currents flowing to a negative probe ($U_p < 0$) are due to collected ions and dust particles. We assume the ions carry one unit of positive elementary charge e, have a mass m_i, and flows supersonically at a speed v_i in the spacecraft reference frame, so that their thermal motion can be ignored and their contribution to the current becomes

$$I_i = -\frac{1}{4} A q_i n_i v_i \left(1 - \frac{2e}{m_i v_i^2} U_p\right), \tag{A2}$$

where A is the surface area of the probe and n_{i} is the ion number density. This result ignores any formation of an ion sheath around the probe, as will be shown reasonable below. This assumption is also further discussed below.

[40] The dust particles are assumed to be so heavy that their kinetic energy is much higher than the range of U_p covered by a probe bias sweep (a few tens of volts). As for the ions, the variation in speed between dust grains is assumed small compared to their bulk speed v_d in the spacecraft frame of reference. The collection of charged dust by the probe then is independent of U_p, and the current carried by the dust is

$$I_d = \frac{1}{4} A e Z n_d v_d, \tag{A3}$$

where n_d is the number density of dust and Z is the average charge of a dust grain. The electron current is ignored, which is permissible for probe potentials lower than a few times the electron temperature due to the exponential decay of the electron current for repelling potentials [e.g., *Wahlund et al.*, 2009].

[41] Assuming that a fraction d of the plasma electrons are bound to dust grains, whose average charge is $-Z\,e$, quasi-neutrality implies the relations

$$q_i n_i = e n_e + e Z n_d, \tag{A4}$$

$$n_e = (1 - \alpha) n_i, \tag{A5}$$

$$n_d = \alpha \frac{n_i}{Z}, \tag{A6}$$

where n_e is the number densities of electrons and $q_i = e$ is assumed.

[42] The sum of (A2) and (A3) obviously describes a current linearly dependent on the probe voltage, as is in fact always observed (Figures 2 and 3). After identification of U_{SC} in the sweep, the quantities directly accessible from the sweep analysis are the offset a and the slope b in the relation

$$I = a + b U_p, \tag{A7}$$

clearly related to the dust and ion parameters (A2) and (A3) by

$$a = \frac{A}{4}(e Z n_d v_d - e n_i v_i) = \frac{A}{4} e n_i v_i (\alpha\beta - 1) \tag{A8}$$

$$b = \frac{A e^2 n_i}{2 m_i v_i}, \tag{A9}$$

where we in (A8) introduced the ratio of dust to ion bulk speed:

$$\beta = \frac{u_d}{u_i}. \tag{A10}$$

In the absence of charged dust, $\acute{a} = 0$, and (A8) and (A9) give

$$v_i = \sqrt{\frac{2e}{m_i}\frac{a}{b}} \equiv v_i', \tag{A11}$$

providing a convenient method for deriving v_i from the observed a and b. In dusty plasmas, where d is nonzero, (A11) evidently modifies to

$$v_i = v_i'/\sqrt{1-\alpha\beta}. \tag{A12}$$

[43] This has some interesting consequences. First, just using v_i' as a measure of ion speed will result in an underestimate of v_i, as $\acute{a}$ and $\hat{a}$ both must take values on the interval [0,1]. Second, some situations can be ruled out directly from comparison to data. One such is the hypothesis that the dust is moving in Keplerian orbits around Saturn while the ions are corotating with the planet. At Enceladus orbit, the Keplerian speed v_K is roughly half the corotation speed v_{corot}, so that $\hat{a} = 0.44$ ($v_K \approx 14.5$ km/s and $v_{\text{corot}} \approx 32.5$ km/s, relative to the spacecraft speed). Inverting (A12), we find that the v_i in this case must have

$$v_i' = \sqrt{0.56}v_{\text{corot}} \approx 0.7 v_{\text{corot}}, \tag{A13}$$

whatever the value of $\acute{a}$. While the data in Figure 5 may possibly be consistent with this at large distances from Enceladus, they certainly are not closer to the moon, where the observed v_i'/v_{corot} goes below 0.4, and the hypothesis can be ruled out here. On the other hand, if the dust is picked up by the corotation electric field so that the dust and the ions orbit Saturn at equal speed, then $\hat{a} = 1$, and (A12) shows that v_i' can be a quite small fraction of the true speed if the dust fraction $\acute{a}$ is high. This explains how it is possible to get values for v_i' below the local Keplerian speed v_K, as is seen for all four data sets in Figure 5 when closest to Enceladus.

A3. Ion Density

[44] The ion density can be derived from the observed parameters a and b in several ways. Multiplying (A8) and (A9) results in an expression for n_i depending only on the observed a and b, the assumed m_i, and the assumed value of $(1 - \acute{a}\hat{a})$. For all these parameters, there is a square root behavior, so small errors in any parameters give an even smaller error in the resulting n_i. If also assuming a value for v_i, one can get the density directly from (A8) or (A9). Using (A9) has the advantage that the dust parameters $\acute{a}$ and $\hat{a}$ are not needed. However, one should note that in all cases, the value of a depends on the value we use for U_{SC}.

[45] We have tried all methods, with quite small differences between them, in no case approaching even a factor of two. We can thus not explain the observed excess of ions over electrons by up to (and even exceeding) a factor of 10 by uncertainties in the ion density. In fact, in the presence of dust, we quite certainly underestimate the ion density, as we assume $\acute{a} = \hat{a} = 0$ when deriving n_i. This has no impact on an estimate based on (A9) alone, but will make us underestimate n_i in any of the other two methods. If anything, the real ion densities are higher than those we report, making the lack of electrons even more conspicuous.

A4. Electron Density

[46] The estimates of electron density n_e discussed in this study derive from the observed electron current at positive bias voltage (Figures 2 and 3) as discussed in section 3.2 and by, e.g., *Wahlund et al.* [2005]. To be more exact, there are two ways of getting n_e: by use of the value of I_{e0} (equation (1)), or by use of the slope of the probe current curve at positive potentials, which is I_{e0}/T_e. The first method is sensitive to errors in the estimate of U_{SC}, as I_{e0} is identified as the current at $U_{\text{bias}} = -U_{\text{SC}}$, while the second is reliable only if the Debye length is large compared to the probe radius so that sheath effects can be neglected [*Laframboise*, 1966]. Both of these methods require an estimate of the electron temperature T_e, which is quite robustly found from the exponential part of the bias sweeps just below $U_{\text{bias}} = -U_{\text{SC}}$, to derive n_e from (1).

[47] There are three potentially significant sources of uncertainty in the n_e estimate: (1) uncertainties in the electron temperature as just discussed, (2) effects of a probe sheath, potentially invalidating the simple expressions from orbital motion limit (OML) probe theory we use, and (3) effects of the spacecraft blocking part of the field of view of the probe and of the negative spacecraft potential, whose extension into space close to the probe can serve to decrease the local electron density. For case 1, the analysis gives consistent and continuously varying T_e values around 1 eV, which is unlikely to be off by more than a factor of two, corresponding to at most a factor 1.4 error in n_e (see equation (1)).

[48] As for possible probe sheath effects (case 2), they could have some effect only in the densest plasma close to Enceladus. Further out, even using the ion density of a few hundred cm^{-3}, the Debye length $\ddot{e}_D > 1$ m. With a probe radius of a 25 mm, $a/\ddot{e}_D \sim 0.05$ or less, which would change the probe current by only a few percent [*Laframboise*, 1966]. Sweeps like in Figure 2 also show a very linear behavior on the positive voltage side, inconsistent with appreciable sheath effects. In the denser region closer to Enceladus, a sweep like in Figure 3 demonstrates a stronger sheath effect, seen as a deviation from linear scaling with voltage for the probe current on the positive voltage side. However, this shielding is not sufficient for explaining the low electron currents we observe: Figure 4 shows a current suppression from the OML result by a factor of around 30 at high probe potentials, which according to numerical simulations could only be achieved for $a/\ddot{e}_D$ on the order of 10^2 or more [*Laframboise*, 1966]. For our case, where $a/\ddot{e}_D$ in the densest case is at most around unity, the expected current suppression compared to OML would be a few tens of percent. The low current we see on the electron side can therefore only to a small extent be attributed to sheath effects: the observed factor of 30 is at least 20 times above what we could explain in this way.

[49] Finally, the satellite potential (case 3) has not decayed to zero at the end of the boom on which the LP is mounted, and this may indeed decrease the electron density in the vicinity of the probe. Particle in cell simulations using a realistic geometric model of Cassini shows that in the limit

of infinite Debye length, almost 80% of the spacecraft potential remains at the probe location, decreasing to 45% for $\ddot{e}_D$ = 74 cm and 28% for $\ddot{e}_D$ = 23 cm [*Nilsson*, 2009]. We can use this in the analytical expressions for the density depletion outside a spherical spacecraft provided by *Laframboise and Godard* [1974], which also includes the effect of spacecraft blocking of part of the electron orbits to the probe. Assuming $U_{SC} \approx -2.5\ KT_e/e$, consistent with, e.g., the sweep data in Figure 2, their equation (8) indicates that the electron density at the probe position can be as low as 13% of the ambient ne if 80% of U_{SC} remains at the probe position. This result depends very weakly on the radius assumed for the sphere representing the spacecraft: varying the ratio of the spacecraft radius to the distance of the probe from the s/c center over a wide range from 0.3 to 0.8 changes the result only from 13.4% to 12.3%, so we can assume 13% to be a good worst case estimate. Using the much lower value for the remaining potential at the probe position quoted above for finite Debye lengths, we get 32% for $\ddot{e}_D$ = 74 cm, relevant for the plasma parameters seen far from Enceladus in Figure 4, while for $\ddot{e}_D$ = 23 cm, relevant for the dense plasmas we infer close to Enceladus, the value is 49%. In conclusion, the absolute worst case limit to this effect would be a factor of 1/0.13 ≈ 8 between sweep-derived ion and electron densities: more realistically, we expect the factor to be 2–3. This could explain the discrepancy between ion and electron densities seen also at the end of the intervals in Figures 4 and 5, but quite certainly not the factor of 20–30 we find close to Enceladus.

[50] In conclusion, we have not been able to explain the observed very large ratio of ion to electron current in any other way than that the electrons are actually missing. We see no other likely mechanism for this than electron attachment to dust grains, particularly as dust is obviously in plentiful supply near Enceladus.

A5. Spacecraft Potential

[51] It may be thought that if a large fraction of the electrons are bound to dust particles, the spacecraft potential must change significantly, perhaps even reaching positive values. We will here show that this only happens if two conditions are met: the fraction of electrons bound to dust must be large, and the dust and ions must have different bulk velocities.

[52] The spacecraft potential is set by the requirement that the total current to the spacecraft should be zero. The time scale for reaching this equilibrium, the RC time of the spacecraft sheath, is on the order of milliseconds, so this balance holds at every moment for the time scales we are interested in. Using the notation of section A2 above with the electron current denoted by I_e, we have

$$I_i + I_d + I_e = 0, \tag{A14}$$

where I_d is given by (A3), with a now representing the radius of the spacecraft, assumed spherical. For the highest densities we see, the Debye length becomes much smaller than the spacecraft size, so (A2) for the ions is replaced by the sheath limited expression

$$I_i = \frac{1}{4} A e n_i v_i. \tag{A15}$$

The electrons are repelled by the spacecraft potential and thus follow

$$I_e = I_{i0} \exp\left(\frac{eU_{SC}}{kT_e}\right), \tag{A16}$$

where I_{e0} is given by equation (1). Solving for the potential gives

$$U_{SC} = \frac{kT_e}{e} \ln\left(\sqrt{\frac{8ekT_e}{\pi m_e}} \frac{1-\alpha}{1-\alpha\beta} v_i\right). \tag{A17}$$

Let us consider the same two cases as discussed in section A2.

A5.1. Case 1: Ions and Dust Both Corotating at the Same Speed

[53] In this case, $\hat{a} = 1$, the dependence on $\acute{a}$ disappears, so that the presence of dust has no impact on the spacecraft potential. This happens because I_i and I_d both depend on density and bulk velocity only, so a fraction $\hat{a}$ of the ion current is exactly canceled by the dust current: the remaining ion fraction $(1 - \acute{a})$ must then be balanced by the electron current from the electrons, whose density is decreased by the same factor $(1 - \acute{a})$ from its value when no dust is present. We thus expect to have $U_{SC} \approx -3.0\ KT_e$/e if we use T_e = 1 eV and v_i = 32.5 km/s (corotation speed) in (A17) and $U_{SC} \approx -3.9\ KT_e/e$ if we use v_i = 14.5 km/s (Keplerian speed).

A5.2. Case 2: Keplerian Dust, Corotating Ions

[54] If we instead consider the case of corotating ions and Keplerian dust ($\hat{a}$ = 0.4, see section A2), U_{SC} will be less negative as the dust fraction increases. For $\acute{a}$ = 0.5 and 0.8, $U_{SC} \approx -2.5$ and $-1.8\ KT_e/e$, respectively, and the spacecraft goes positive when $\acute{a} \approx 0.97$.

[55] From the observed electron temperatures and consistently negative spacecraft potentials, on the order of what we expect in case 1, it is clear that case 2 can be ruled out at least for the highest dust fractions. This can be considered independent evidence for rapid pickup of charged dust.

[56] **Acknowledgments.** The Swedish National Space Board (SNSB) supports the RPWS/LP instrument on board Cassini, and the research at the University of Iowa is supported by a NASA contract.

[57] Masaki Fujimoto thanks the reviewers for their assistance in evaluating this paper.

References

Arridge, C. S., K. K. Khurana, C. T. Russell, D. J. Southwood, N. Achilleos, M. K. Dougherty, A. J. Coates, and H. K. Leinweber (2008), Warping of Saturn's magnetospheric and magnetotail current sheets, *J. Geophys. Res.*, *113*, A08217, doi:10.1029/2007JA012963.

Barkan, A., N. D'angelo, and R. Merlino (1994), Charging of dust grains in a plasma, *Phys. Rev. Lett.*, *73*, 3093–3096, doi:10.1103/PhysRevLett.73.3093.

Blanc, M. F., R. Kallenbach, and N. V. Erkaev (2005), Solar system magnetospheres, *Space Sci. Rev.*, *116*, 227–298, doi:10.1007/s11214-005-1958-y.

Burch, J. L., J. Goldstein, P. Mokashi, W. S. Lewis, C. Paty, D. T. Young, A. J. Coates, M. K. Dougherty, and N. André (2008), On the cause of Saturn's plasma periodicity, *Geophys. Res. Lett.*, *35*, L14105, doi:10.1029/2008GL034951.

Burton, M. E., M. K. Dougherty, and C. T. Russell (2009), Model of Saturn's internal planetary magnetic field based on Cassini observations, *Planet. Space Sci.*, *57*, 1706–1713, doi:10.1016/j.pss.2009.04.008.

Desch, M. D., and M. L. Kaiser (1981), Voyager measurement of the rotation period of Saturn's magnetic field, *Geophys. Res. Lett.*, *8*, 253–256, doi:10.1029/GL008i003p00253.

Dougherty, M. K., K. K. Khurana, F. M. Neubauer, C. T. Russell, J. Saur, J. S. Leisner, and M. E. Burton (2006), Identification of a dynamic atmosphere at Enceladus with the Cassini magnetometer, *Science*, *311*, 1406–1409, doi:10.1126/science.1120985.

Espinosa, S. A., D. J. Southwood, and M. K. Dougherty (2003), How can Saturn impose its rotation period in a noncorotating magnetosphere? *J. Geophys. Res.*, *108*(A2), 1086, doi:10.1029/2001JA005084.

Farrell, W. M., W. S. Kurth, D. A. Gurnett, R. E. Johnson, M. L. Kaiser, J.-E. Wahlund, and H. Waite Jr. (2009), Electron density dropout near Enceladus in the context of water-vapor and water-ice, *Geophys. Res. Lett.*, *36*, L10203, doi:10.1029/2008GL037108.

Farrell, W. M., W. S. Kurth, R. L. Tokar, J.-E. Wahlund, D. A. Gurnett, Z. Wang, R. J. MacDowall, M. W. Morooka, R. E. Johnson, and H. Waite Jr. (2010), Modification of the plasma in the near-vicinity of Enceladus by the enveloping dust, *Geophys. Res. Lett.*, *37*, L20202, doi:10.1029/2010GL044768.

Giampieri, G., M. K. Dougherty, E. J. Smith, and C. T. Russell (2006), A regular period for Saturn's magnetic field that may track its internal rotation, *Nature*, *441*, 62–64, doi:10.1038/nature04750.

Goertz, C. K. (1989), Dusty plasmas in the solar system, *Rev. Geophys.*, *27*, 271–292, doi:10.1029/RG027i002p00271.

Goertz, C. K., M. F. Thomsen, and W.-H. Ip (1981), Saturn's radio emissions: Rotational modulation, *Nature*, *292*, 737–739, doi:10.1038/292737a0.

Gurnett, D. A., and A. Bhattacharjee (2005), *Introduction to Plasma Physics With Space and Laboratory Applications*, Cambridge Univ. Press, Cambridge, U. K.

Gurnett, D. A., et al. (2004), The Cassini radio and plasma wave investigation, *Space Sci. Rev.*, *114*, 395–463, doi:10.1007/s11214-004-1434-0.

Gurnett, D. A., A. M. Persoon, W. S. Kurth, J. B. Groene, T. F. Averkarnp, M. K. Dougherty, and D. J. Southwood (2007), The variable rotation period of the inner region of Saturn's plasma disk, *Science*, *316*, 442–445, doi:10.1126/science.1138562.

Hall, A. (1877), On the rotation of Saturn, *Astron. Nachr.*, *90*, 145–150, doi:10.1002/asna.18770901002.

Havnes, O., K. Aanesen, and F. Melandsø (1990), On dust charges and plasma potentials in a dusty plasma with dust size distribution, *J. Geophys. Res.*, *95*, 6581–6585, doi:10.1029/JA095iA05p06581.

Havnes, O., L. I. Næsheim, T. W. Hartquist, G. E. Morfill, F. Melandsø, B. Schleicher, J. Trøim, T. Blix, and E. Thrane (1996), Meter-scale variations of the charge carried by mesospheric dust, *Planet. Space Sci.*, *44*, 1191–1194, doi:10.1016/S0032-0633(96)00041-4.

Horányi, M. (1996), Charged dust dynamics in the solar system, *Annu. Rev. Astron. Astrophys.*, *34*, 383–418, doi:10.1146/annurev.astro.34.1.383.

Horányi, M., T. W. Hartquist, O. Havnes, D. A. Mendis, and G. E. Morfill (2004), Dusty plasma effects in Saturn's magnetosphere, *Rev. Geophys.*, *42*, RG4002, doi:10.1029/2004RG000151.

Jones, G. H., et al. (2009), Fine jet structure of electrically charged grains in Enceladus' plume, *Geophys. Res. Lett.*, *36*, L16204, doi:10.1029/2009GL038284.

Kempf S., U. Beckmann, R. Srama, M. Horanyi, S. Auer, and E. Grün (2006), The electrostatic potential of E ring particles, *Planet. Space Sci.*, *54*, 999–1006, doi:10.1016/j.pss.2006.05.012.

Kempf, S., U. Beckmann, G. Moragas-Klostermeyer, F. Postberg, R. Srama, T. Economou, J. Schmidt, F. Spahn, and E. Gruen (2008), The E ring in the vicinity of Enceladus—I. Spatial distribution and properties of the ring particles, *Icarus*, *193*, 420–437, doi:10.1016/j.icarus.2007.06.027.

Khurana, K. K., D. G. Mitchell, C. S. Arridge, M. K. Dougherty, C. T. Russell, C. Paranicas, N. Krupp, and A. J. Coates (2009), Sources of rotational signals in Saturn's magnetosphere, *J. Geophys. Res.*, *114*, A02211, doi:10.1029/2008JA013312.

Kurth, W. S., T. F. Averkarnp, D. A. Gurnett, and Z. Wang (2006), Cassini RPWS observations of dust in Saturn's E Ring, *Planet. Space Sci.*, *54*, 988–998, doi:10.1016/j.pss.2006.05.011.

Kurth, W. S., T. F. Averkarnp, D. A. Gurnett, A. Lecacheux, and J. B. Groene (2008), An update to a Saturnian longitude system based on kilometric radio emissions, *J. Geophys. Res.*, *113*, A05222, doi:10.1029/2007JA012861.

Laframboise, J. G. (1966), *Theory of Spherical and Cylindrical Langmuir Probes in a Collisionless Maxwellian Plasma at Rest*, Inst. for Aerosp. Stud., Univ. of Toronto, Toronto, Ont., Canada.

Laframboise, J. G., and R. Godard (1974), Perturbation of an electrostatic probe by a spacecraft at small speed ratios, *Planet. Space Sci.*, *22*, 1145–1155, doi:10.1016/0032-0633(74)90069-5.

Morooka, M. W., et al. (2009), The electron density of Saturn's magnetosphere, *Ann. Geophys.*, *27*, 2971–2991, doi:10.5194/angeo-27-2971-2009.

Nilsson, T. (2009), Modelling of Cassini Langmuir probe measurements, report, Swed. Inst. of Space Phys., Uppsala, and Dept. of Phys. and Astron., Uppsala Univ., Uppsala, Sweden.

Persoon, A. M., D. A. Gurnett, W. S. Kurth, G. B. Hospodarsky, J. B. Groene, P. Canu, and M. K. Dougherty (2005), Equatorial electron density measurements in Saturn's inner magnetosphere, *Geophys. Res. Lett.*, *32*, L23105, doi:10.1029/2005GL024294.

Porco, C., P. Helfenstein, P. C. Thomas, A. P. Ingersoll, J. Wisdom, R. A. West, G. Neukum, T. Denk, R. Wagner, and T. Roatsch (2006), Cassini observes the active south pole of Enceladus, *Science*, *311*, 1393–1401, doi:10.1126/science.1123013.

Read, P. L., T. E. Dowling, and G. Schubert (2009), Saturn's rotation period from its atmospheric planetary-wave configuration, *Nature*, *460*, 608–610, doi:10.1038/nature08194.

Richardson, J. D., A. Eviatar, M. A. McGrath, and V. M. Vasyliũnas (1998), OH in Saturn's magnetosphere: Observations and implications, *J. Geophys. Res.*, *103*, 20,245–20,255, doi:10.1029/98JE01127.

Shemansky, D. E., P. Matheson, D. T. Hall, H.-Y. Hu, and T. M. Tripp (1993), Detection of the hydroxy radical in the Saturn magnetosphere, *Nature*, *363*, 329–331, doi:10.1038/363329a0.

Shukla, P. K. (2001), A survey of dusty plasma physics, *Phys. Plasmas*, *8*, 1791–1804, doi:10.1063/1.1343087.

Shukla, P. K., and B. Eliasson (2009), Colloquium: Fundamentals of dust-plasma interactions, *Rev. Mod. Phys.*, *81*, 25–44, doi:10.1103/RevModPhys.81.25.

Shukla, P. K., and A. A. Mamun (2002), *Introduction to Dusty Plasma Physics*, IoP, London.

Simon, S., J. Saur, H. Kriegel, F. M. Neubauer, U. Motschmann, and M. K. Dougherty (2011), Influence of negatively charged plume grains and hemisphere coupling currents on the structure of Enceladus' Alfvén wings: Analytical modeling of Cassini magnetometer observations, *J. Geophys. Res.*, *116*, A04221, doi:10.1029/2010JA016338.

Spahn, F., J. Schmidt, N. Albers, M. Horning, M. Makuch, M. Seiss, S. Kempf, R. Srama, V. V. Dikarev, and S. Helfert (2006), Cassini dust measurements at Enceladus and implications for the origin of the E ring, *Science*, *311*, 1416–1418, doi:10.1126/science.1121375.

Tokar, R. L., R. E. Johnson, M. F. Thomsen, R. J. Wilson, D. T. Young, F. J. Crary, A. J. Coates, G. H. Jones, and C. S. Paty (2009), Cassini detection of Enceladus's cold water-group plume ionosphere, *Geophys. Res. Lett.*, *36*, L13203, doi:10.1029/2009GL038923.

Wahlund, J.-E., et al. (2005), The inner magnetosphere of Saturn-Cassini RPWS cold plasma results from the first encounter, *Geophys. Res. Lett.*, *32*, L20S09, doi:10.1029/2005GL022699.

Wahlund, J.-E., et al. (2009), Detection of dusty plasma near the E-ring of Saturn, *Planet. Space Sci.*, *57*, 1795–1806, doi:10.1016/j.pss.2009.03.011.

Waite, J. H., Jr., M. R. Combi, W. H. Ip, T. E. Cravens, R. L. McNutt Jr., W. Kasprzak, R. Yelle, J. Luhmann, H. Niemann, and D. Gell (2006), Cassini ion and neutral mass spectrometer: Enceladus plume composition and structure, *Science*, *311*, 1419–1422, doi:10.1126/science.1121290.

Wang, Z., D. A. Gurnett, T. F. Averkarnp, A. M. Persoon, and W. S. Kurth (2006), Characteristics of dust particles detected near Saturn's ring plane with the Cassini Radio and Plasma Wave instrument, *Planet. Space Sci.*, *54*, 957–966, doi:10.1016/j.pss.2006.05.015.

Wilson, R. J., R. L. Tokar, M. G. Henderson, T. W. Hill, M. F. Thomsen, and D. H. Pontius (2008), Cassini plasma spectrometer thermal ion measurements in Saturn's inner magnetosphere, *J. Geophys. Res.*, *113*, A12218, doi:10.1029/2008JA013486.

Yaroshenko, V. V., S. Ratynskaia, J. Olson, N. Brenning, J.-E. Wahlund, M. W. Morooka, W. S. Kurth, D. A. Gurnett, and G. E. Morfil (2009), Characteristics of charged dust inferred from the Cassini RPWS measurements in the vicinity of Enceladus, *Planet. Space Sci.*, *57*, 1807–1812.

Young, D. T., et al. (2005), Composition and dynamics of plasma in Saturn's magnetosphere, *Science*, *307*, 1262–1266, doi:10.1126/science.1106151.

M. André, A. I. Eriksson, M. K. G. Holmberg, M. W. Morooka, M. Shafiq, and J.-E. Wahlund, Swedish Institute of Space Physics, PO Box 537, SE-75121 Uppsala, Sweden. (morooka@irfu.se)

W. M. Farrell, Planetary Magnetospheres Laboratory, Goddard Space Flight Center, Code 695, Greenbelt, MD 20771, USA.

D. A. Gurnett, W. S. Kurth, and A. M. Persoon, Department of Physics and Astronomy, University of Iowa, Iowa City, IA 52242, USA.